Stanford Exploration Project, Report 100, April 20, 1999, pages 257–269

3-D traveltime computation by Huygens wavefront tracing

Paul Sava[1]

keywords: *finite differences, traveltimes, eikonal, Huygens*

ABSTRACT

In this paper, I present a 3-D implementation of Huygens wavefront tracing. The three-dimensional version of the method retains the characteristics of the two-dimensional one: stability, accuracy, and efficiency. The major difficulty of the 3-D extension is related to the handling of triplications. An easy to implement solution is to approximate the wavefronts at the triplications as planes orthogonal to the incident ray.

INTRODUCTION

The goal of obtaining efficient and robust multiple-arrival traveltimes has yet to be accomplished in practice. The typical traveltime methods–eikonal solvers, ray tracing and wavefront construction–either only compute the first-arrival traveltimes (eikonal solvers) or are expensive and not always robust in regions of high velocity variation (ray tracing and wavefront construction). However, Huygens wavefront tracing (HWT), introduced in a previous paper (Sava and Fomel, 1998), does offer a robust and very efficient method of computing multiple-arrival traveltimes.

This paper presents my extension of Huygens wavefront tracing to three dimensions. I start by briefly reviewing the theory, then I discuss how to handle the triplications of the wavefronts and present one 2-D and two 3-D examples. I continue with a brief comparison to other traveltime methods, and end with conclusions and possible directions for future work.

REVIEW OF HWT THEORY

Given an isotropic heterogeneous medium, wavefronts are represented by surfaces of equal traveltime, constrained by the eikonal equation

$$\left(\frac{\partial \tau}{\partial x}\right)^2 + \left(\frac{\partial \tau}{\partial y}\right)^2 + \left(\frac{\partial \tau}{\partial z}\right)^2 = \frac{1}{v^2(x,y,z)} \tag{1}$$

[1]**email:** paul@sep.stanford.edu

and appropriate boundary conditions.

Each point on a wavefront can be parametrized by either its Cartesian coordinates x, y, and z, or its ray coordinates, which consist of the traveltime τ, and the two shooting angles at the source, γ and ϕ.

For complex velocity fields, the ray coordinates as a function of the Cartesian coordinates become multi-valued, in other words, there is more than one ray going through a given point in the subsurface. In contrast, the Cartesian coordinates as a function of the ray coordinates remain single-valued, that is, there is one unique position in the subsurface where a ray, shot with two particular shooting angles, arrives at a given time. Figure 1 illustrates the difference between the two representations of the wavefronts.

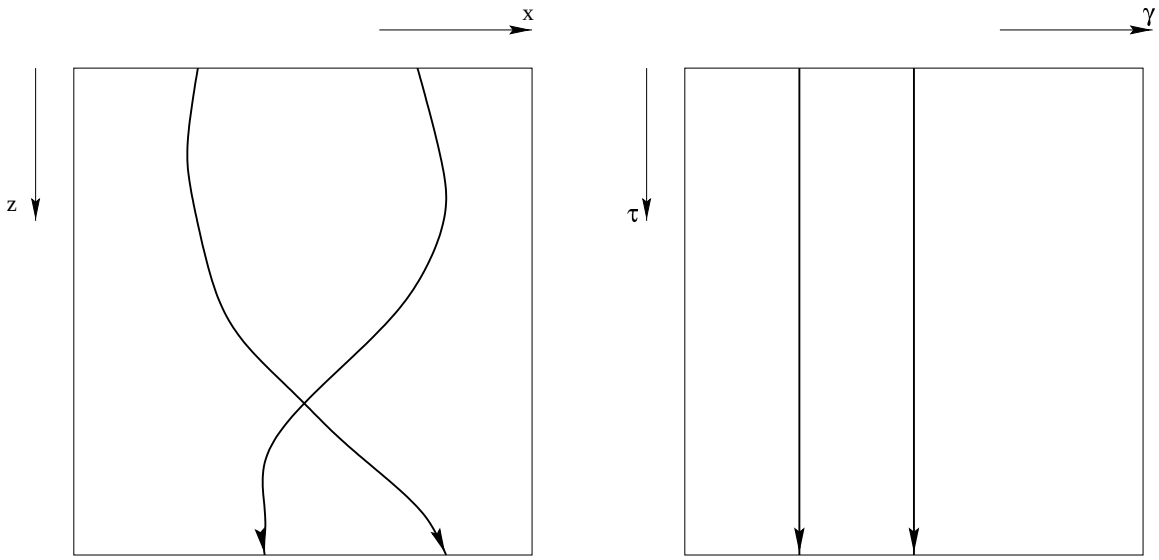

Figure 1: The ray coordinates as a function of the Cartesian coordinates are multi-valued (left). The Cartesian coordinates as a function of the ray coordinates are single-valued (right). paul2-coord [NR]

Since $x(\tau, \gamma, \phi)$, $y(\tau, \gamma, \phi)$, and $z(\tau, \gamma, \phi)$ are uniquely defined for arbitrarily complex velocity fields, the eikonal equation (Equation 1) can be transformed to another form that is better suited for analysis in ray coordinates (Sava and Fomel, 1998):

$$\left(\frac{\partial x}{\partial \tau}\right)^2 + \left(\frac{\partial y}{\partial \tau}\right)^2 + \left(\frac{\partial z}{\partial \tau}\right)^2 = v^2(x, y, z)\,. \tag{2}$$

Converting equation (2) to a finite-difference equation using a first-order discretization scheme, we obtain

$$\left(x_{j+1}^{i,k} - x_j^{i,k}\right)^2 + \left(y_{j+1}^{i,k} - y_j^{i,k}\right)^2 + \left(z_{j+1}^{i,k} - z_j^{i,k}\right)^2 = \left(r_j^{i,k}\right)^2\,, \tag{3}$$

where j is the index of the current wavefront, $j+1$ is the index of the new wavefront to be computed, and i and k are the indices of the shooting angles. This equation represents

a sphere, the wavefront of a secondary Huygens source placed at $(x_j^{i,k}, y_j^{i,k}, z_j^{i,k})$ on the current wavefront.

According to the Huygens principle, the new wavefront is the envelope of all the secondary wavefronts. Mathematically, the position of the new wavefront is described by a system of three equations composed of Equation (3) and the following two equations (Sava and Fomel, 1998):

$$\left(x_j^{i,k} - x_{j+1}^{i,k}\right)\left(x_j^{i+1,k} - x_j^{i-1,k}\right) + \left(y_j^{i,k} - y_{j+1}^{i,k}\right)\left(y_j^{i+1,k} - y_j^{i-1,k}\right) + \left(z_j^{i,k} - z_{j+1}^{i,k}\right)\left(z_j^{i+1,k} - z_j^{i-1,k}\right) = r_j^{i,k}\left(r_j^{i+1,k} - r_j^{i-1,k}\right) \tag{4}$$

and

$$\left(x_j^{i,k} - x_{j+1}^{i,k}\right)\left(x_j^{i,k+1} - x_j^{i,k-1}\right) + \left(y_j^{i,k} - y_{j+1}^{i,k}\right)\left(y_j^{i,k+1} - y_j^{i,k-1}\right) + \left(z_j^{i,k} - z_{j+1}^{i,k}\right)\left(z_j^{i,k+1} - z_j^{i,k-1}\right) = r_j^{i,k}\left(r_j^{i,k+1} - r_j^{i,k-1}\right) . \tag{5}$$

Figure 2 contains a simple geometrical interpretation of the system described by Equations (3), (4), and (5). Five points on the current wavefront, represented by the five spheres, not all visible, with radii defined by the velocities at the corresponding points of the wavefront, are used to compute a point on the next wavefront. The sphere in the middle represents equation (3), while the planes represent equations (4) and (5).

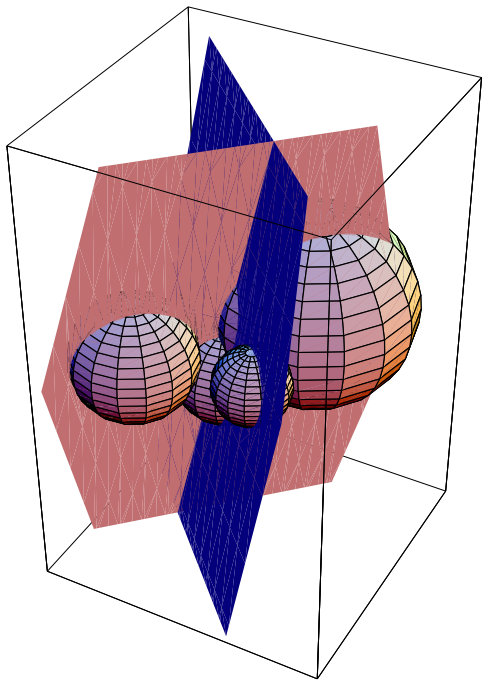

Figure 2: A geometrical updating scheme for 3-D HWT in the physical domain. Five points on the current wavefront, represented by the five spheres, not all visible, with radii defined by the velocities at the corresponding points of the wavefront, are used to compute a point on the next wavefront. The sphere in the middle represents equation (3), and the planes represent equations (4) and (5). paul2-huygens3d [CR]

Huygens wavefront tracing, based on the system of equations (3), (4), and (5), is nothing but an explicit finite-difference method in the ray coordinate system. The coordinates of the new wavefronts are computed according to those of the current wavefront. A three-point stencil is needed in two dimensions to compute the centered finite-difference representation

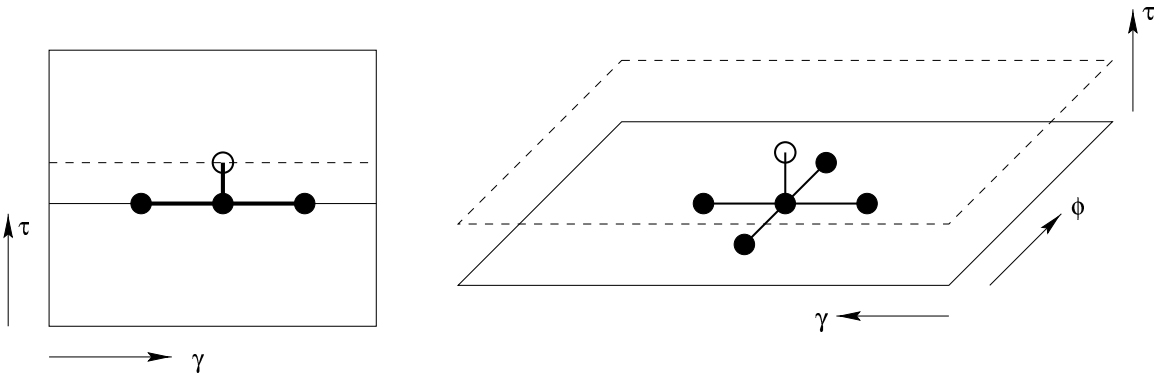

Figure 3: Finite-difference traveltime computation scheme. A 3-point stencil is needed in 2-D to compute the centered finite-difference representation of the derivative with respect to the shooting angle (left). A 5-point stencil is needed in 3-D to compute the centered finite-difference representation of the derivatives with respect to the shooting angles (right) paul2-scheme [NR]

of the derivative with respect to the shooting angle, while a five-point stencil is needed in three dimensions to compute the centered finite-difference representation of the derivatives with respect to the shooting angles. Figure 3 is a graphical illustration of the finite-difference stencils.

BOUNDARIES AND TRIPLICATIONS

This section presents a short discussion of the special treatment required by the boundaries of the computation domain. These boundaries are of two kinds: exterior boundaries, represented by the edges of the computational domain, and interior boundaries, represented by the triplication lines. Because of the centered finite-difference scheme, HWT cannot be used at the boundaries of the computational domain. This means that the boundaries need to be treated differently from the rest of the domain. Also, the centered finite-difference scheme cannot be used when the wavefronts create triplications. Triplications represent points of discontinuity of the derivative along the wavefront, and, therefore, the centered finite-difference representation of the derivative is inappropriate. Figure 4 describes a point of triplication represented in both the physical (Cartesian) domain (left) and the ray coordinate domain (right).

One possible solution for the boundaries is to make a local approximation of the wavefront. Instead of considering the actual points on the wavefront, we can create an approximate wavefront that is locally orthogonal to the ray arriving at the cusp point, as depicted in Figure 5. We can then pick an appropriate number of points (two in 2-D or four in 3-D) on this approximate wavefront, and use the HWT scheme without any change. A new search for the cusp points is then needed on the new wavefront before we can proceed any further.

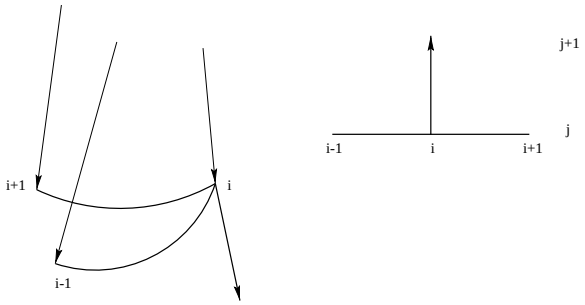

Figure 4: The centered finite-difference representation of the derivative along the wavefront cannot be used at the cusps. These points represent discontinuities in the derivative, and need to be treated separately. paul2-cusp [NR]

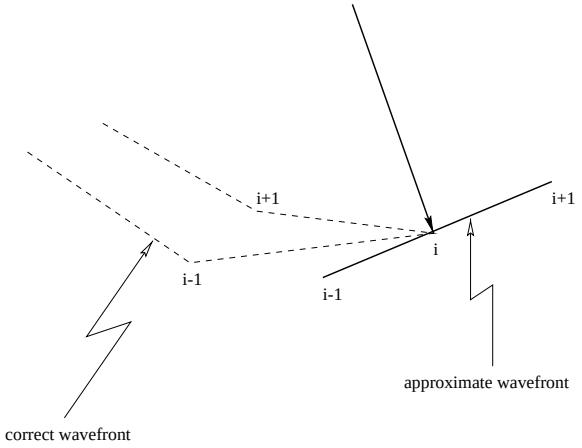

Figure 5: The centered finite-difference representation of the derivative along the wavefront cannot be used at the cusps. Instead, we can use a local approximation of the wavefront as a plane locally orthogonal to the ray arriving at the cusp. paul2-hrt [NR]

EXAMPLES

This section presents a number of results of traveltime computation using several models that exemplify the main features of the method.

The first example compares the results of the traveltime computation with those of the full wave-equation modeling for the 2-D salt dome model shown in Figure 6. Figure 7 is a snapshot of the wavefield at 1.23 s, superimposed on an outline of the velocity model. Figure 8 shows, in addition, the wavefront corresponding to the same propagation time (1.23s), and some of the rays derived from the computed wavefronts. The first arrivals of the wavefronts superimpose well on the similar events in the wavefield. The later arrivals also superimpose well on the corresponding events in the wavefield, though the sampling is a lot sparser. This is understandable, since in HWT the wavefronts are sampled evenly in the ray domain, but not in the physical domain. Because sampling in the two domains is related, a better sampling in the ray domain can generate more accurate sampling in the physical domain. However, sampling is dependent on the model; there is no guarantee of more accurate sampling for rays shot with a smaller angle step. A better idea is to dynamically modify the sampling on the wavefronts as is done in some of the wavefront construction methods (Vinje et al., 1993).

The next two examples are three-dimensional. In the first, I consider a strong negative Gaussian velocity anomaly of -2500 m/s placed in a constant velocity medium of 3000 m/s (Figure 9). The source is placed on the surface above the center of the anomaly. Figure 11

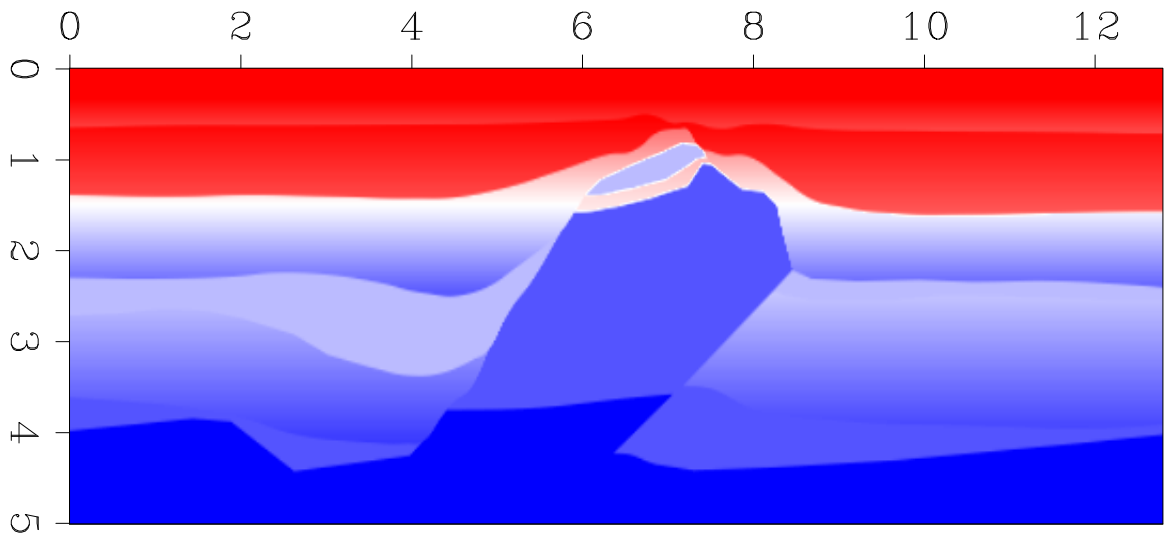

Figure 6: The Elf velocity model. paul2-velfsa [ER]

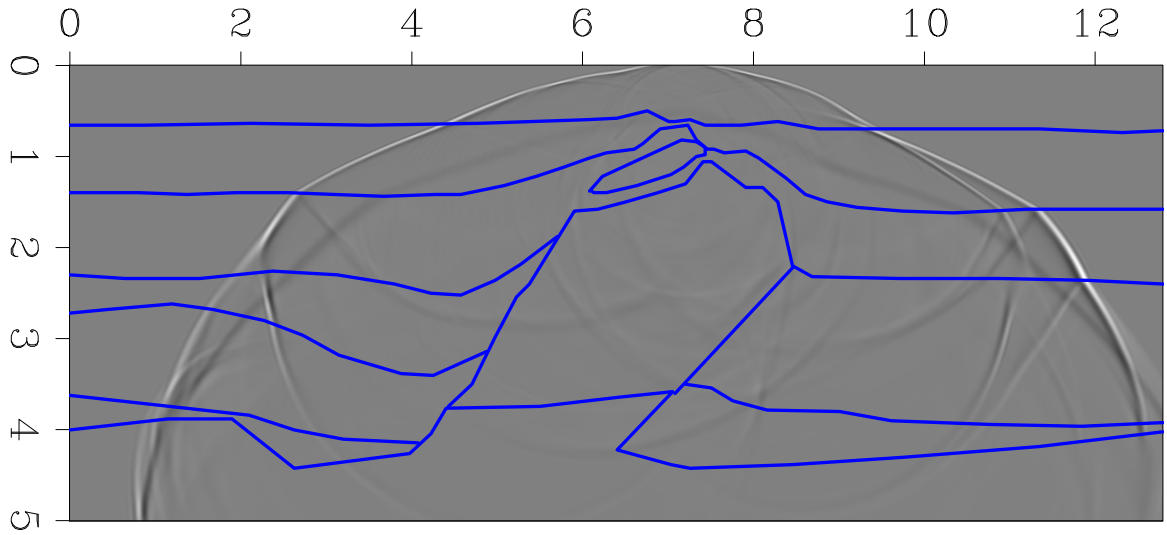

Figure 7: Wave-equation modeling on the Elf velocity model. The snapshot was taken at 1.23s. The outline on the model is superimposed on the wavefield. paul2-melfsa [ER]

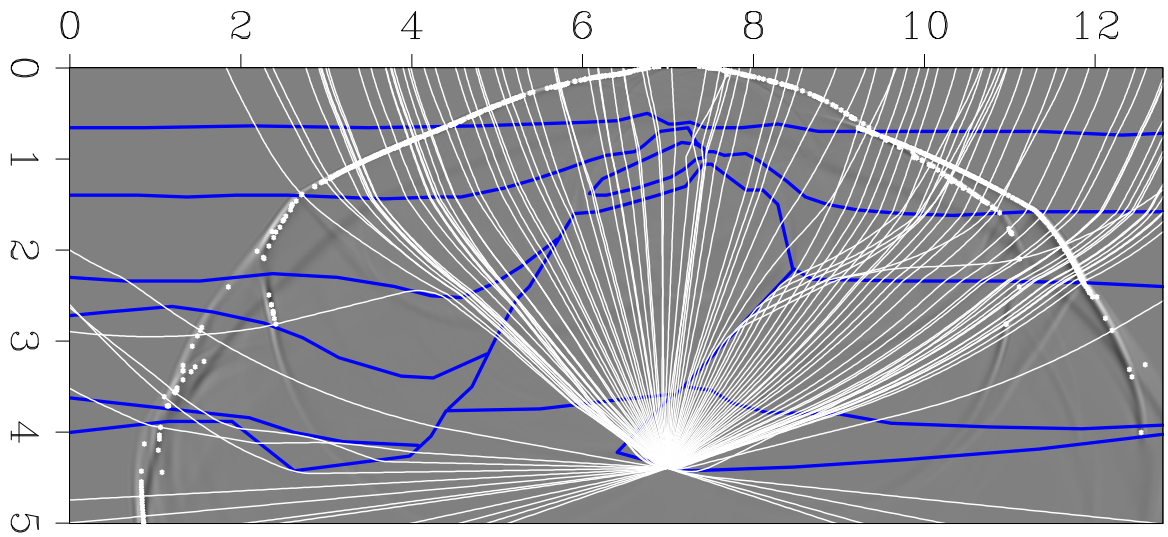

Figure 8: HWT wavefront superimposed on a wave-equation modeling snapshot at 1.23s. The portion of the wavefronts corresponding to the first-arrival matches well the first-arrival of the wavefield. Also, the later HWT arrivals match well with similar events of the wave-equation modeling shown in Figure 7. paul2-welfsa [ER]

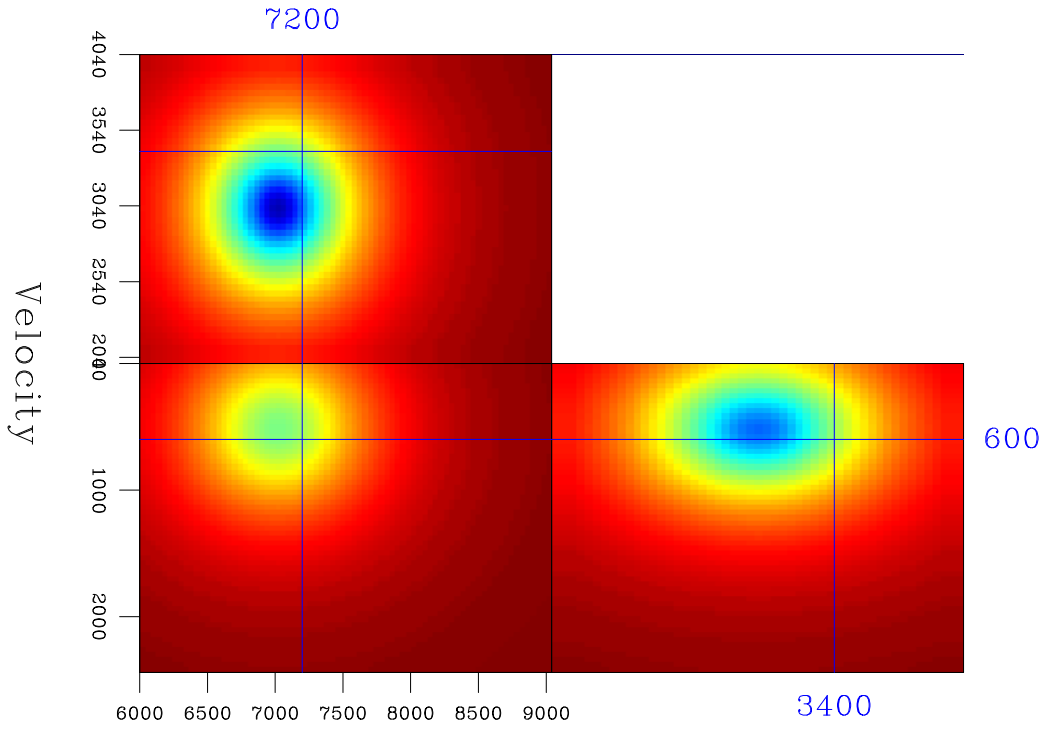

Figure 9: A 3-D Gaussian velocity anomaly. paul2-velgaus [ER]

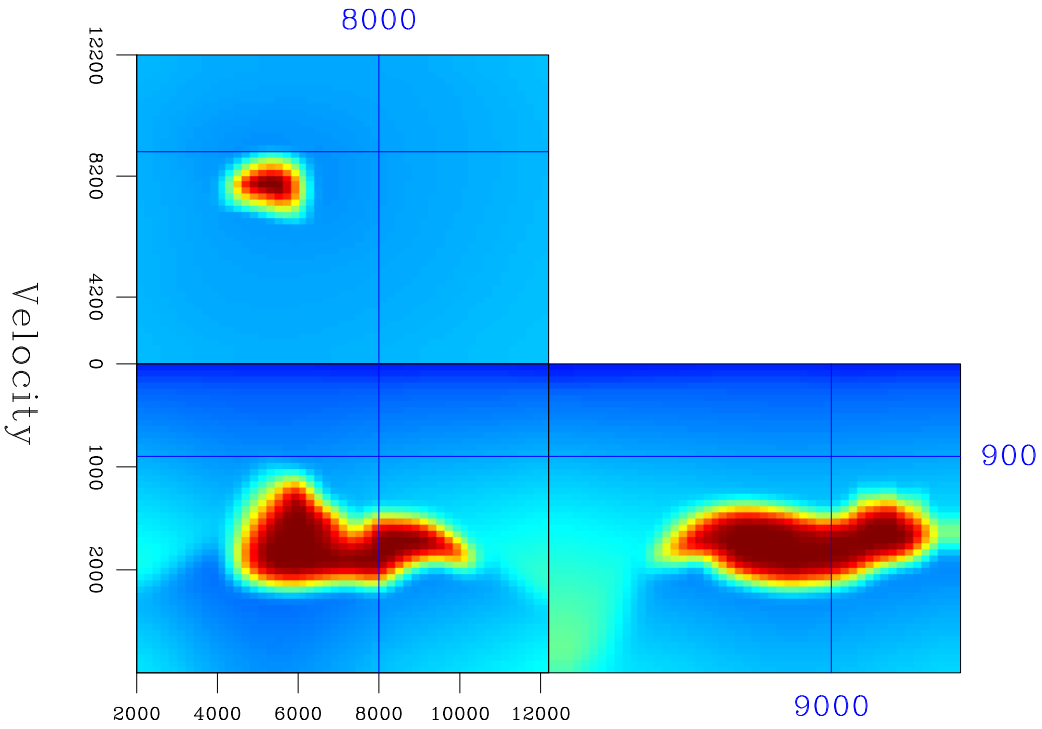

Figure 10: The 3-D SEG-EAGE salt velocity model. paul2-velsalt [ER]

depicts the traveltimes obtained by HWT and interpolated on the Cartesian grid using a multi-valued traveltime interpolation method (Sava and Biondi, 1997). From the multiple values of the traveltime field, I have selected those that correspond to the minimum ray-length from the source (Nichols et al., 1998). For comparison, Figure 12 indicates the first-arrival traveltimes of a fast marching eikonal solver (FME) (Popovici and Sethian, 1997; Fomel, 1997). As expected, the traveltime cubes in Figures 11 and 12 match well for the regions that correspond to the first-arrival wavefronts. However, the traveltime cubes are completely different in the regions where the wavefronts triplicate, regions where the shortest ray does not correspond to the first arrival, but to a later one.

In the second 3-D example, I consider the SEG-EAGE salt model presented in Figure 10. Again, the HWT multiple-arrival traveltimes are interpolated on the Cartesian grid, and selected to have the minimum ray-length from the source, as we see in Figure 13. For comparison, the fast-marching eikonal results for the same source point and the same velocity model appear in Figure 14. The HWT traveltimes for the volume above the salt body correspond to the direct arrival, while the FME traveltimes correspond to the head waves from the top of the salt.

DISCUSSION

This section briefly compares Huygens wavefront tracing with the other major traveltime computation methods: paraxial ray tracing (PRT) (Červený, 1987), eikonal solvers (ES)

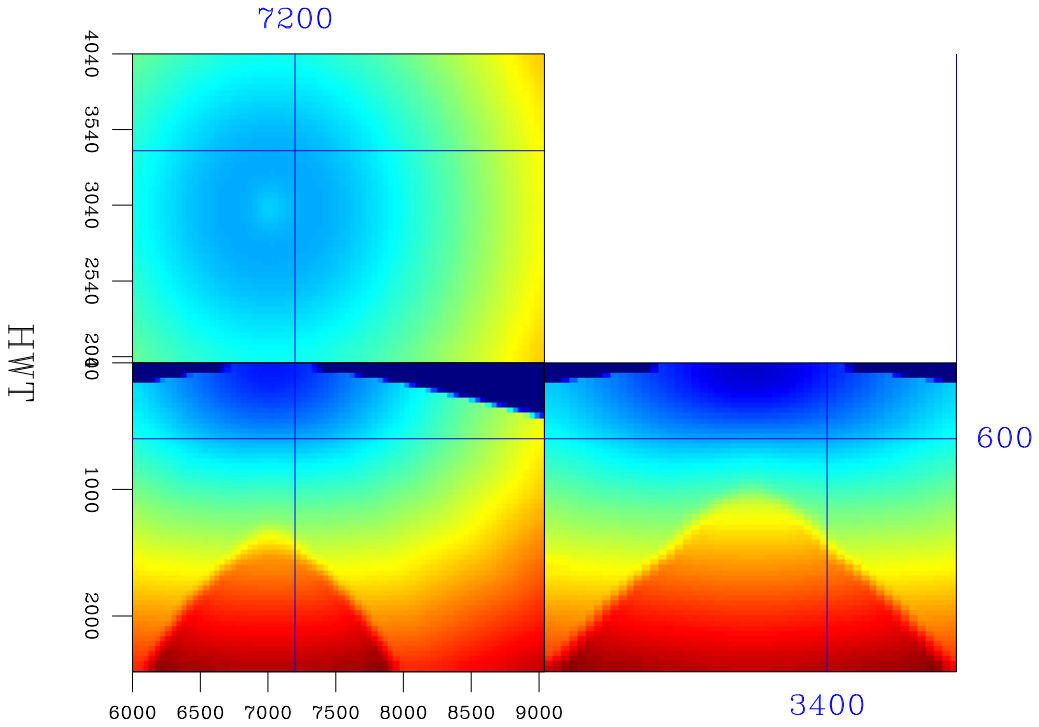

Figure 11: The 3-D Gaussian velocity anomaly. A traveltime cube obtained using HWT. The traveltimes are interpolated on the rectangular grid. The selected traveltimes correspond to the shortest rays (Nichols et al., 1998). paul2-hwtgaus [ER]

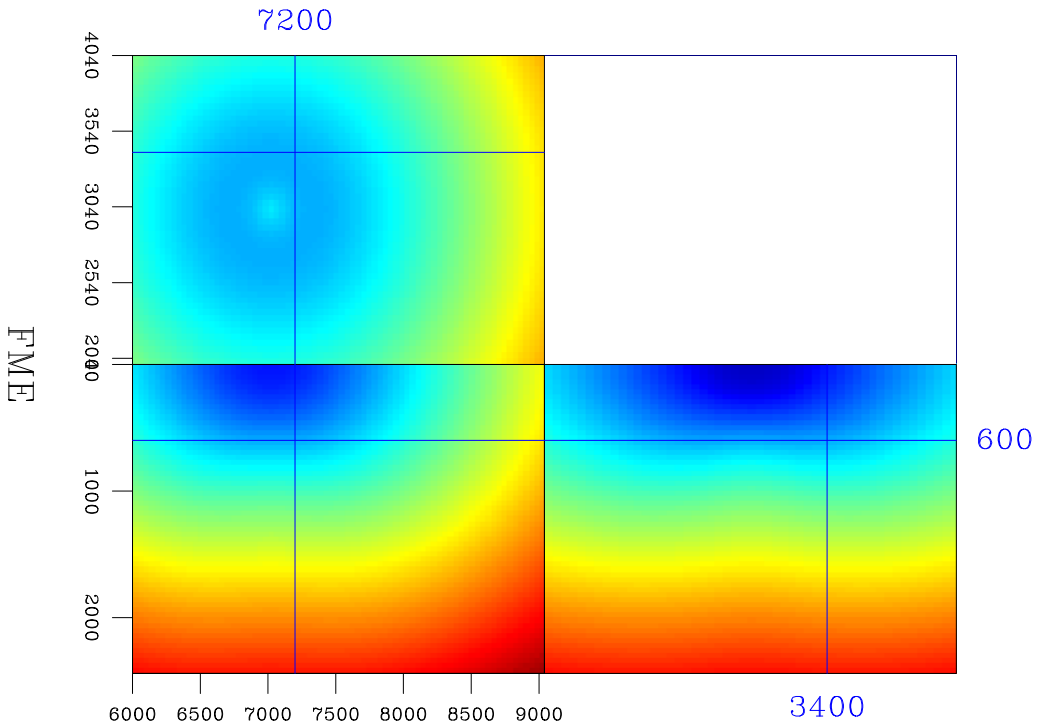

Figure 12: The 3-D Gaussian velocity anomaly. A traveltime cube obtained using a fast-marching first-arrival eikonal solver. paul2-fmegaus [ER]

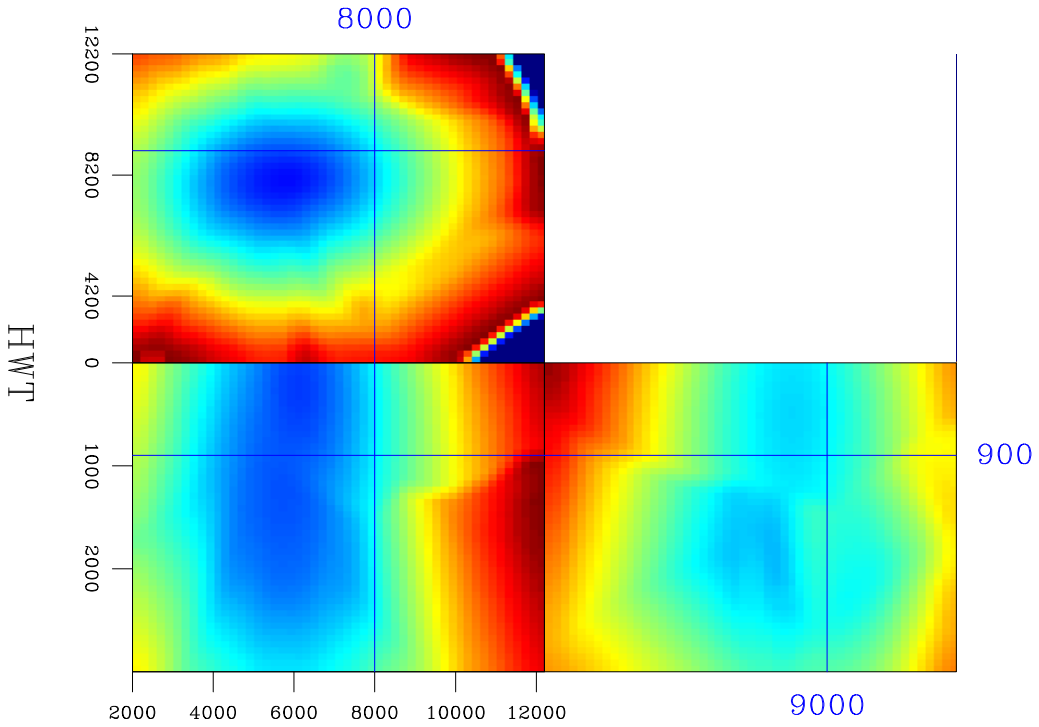

Figure 13: The SEG-EAGE salt model. A traveltime cube obtained using HWT. The traveltimes are interpolated on the rectangular grid. The selected traveltimes correspond to the shortest path rays. paul2-hwtsalt [ER]

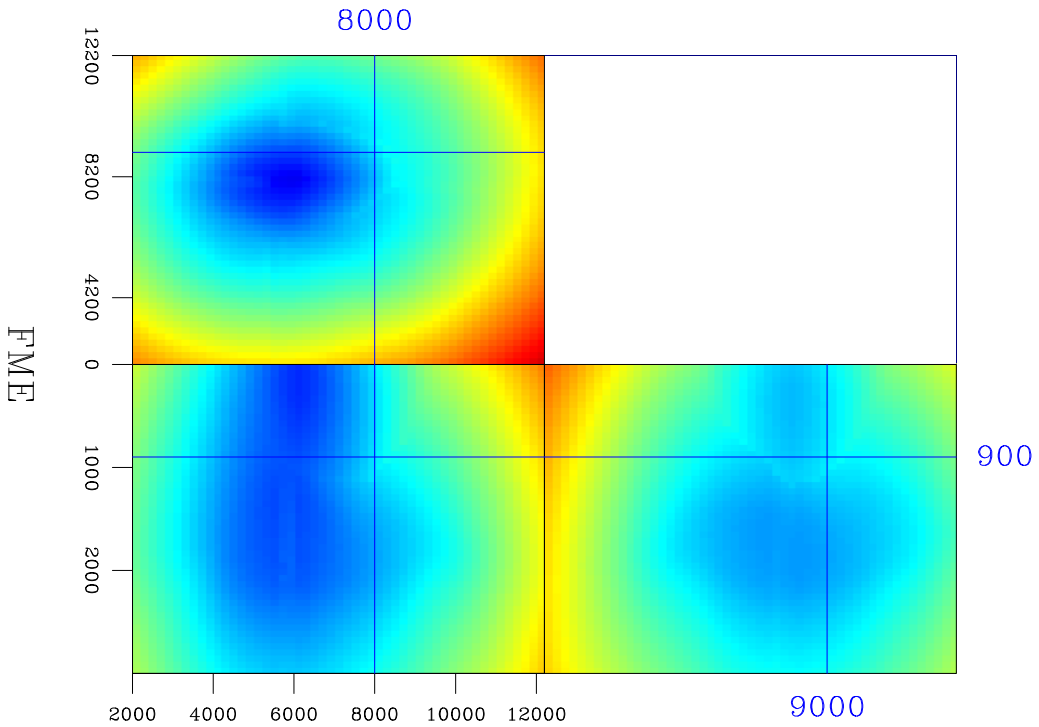

Figure 14: The SEG-EAGE salt model. A traveltime cube obtained using a fast-marching first-arrival eikonal solver. paul2-fmesalt [ER]

Table 1: Comparison of methods for traveltime computation

Wavefront Tracing finds the solution to a system of PDEs	**Ray Tracing** finds the solution to a system of ODEs
Wavefront Tracing gives the output in ray coordinates computes multiple arrivals	**Eikonal Solvers** gives the output in Cartesian coordinates computes one arrival
Wavefront Tracing finds a new wavefront by finite-differences	**Wavefront Construction** finds a new wavefront by ray tracing

(Vidale, 1990; van Trier and Symes, 1991; Popovici and Sethian, 1997; Fomel, 1997), and wavefront construction (WC) (Vinje et al., 1993). Table 1 summarizes the comparison.

HWT has its output in ray coordinates, the same domain as PRT. However, PRT is done by solving a system of ordinary differential equations (ODE) in the physical domain, while in HWT the solution is obtained by solving a system of partial differential equations (PDE) using finite-differences in the ray coordinate domain.

Both HWT and ES are finite-difference methods. However, HWT represents a finite-difference method in the ray domain, while ES represent finite-difference methods in the Cartesian domain. Also, HWT generates all the arrivals, while the ES generate only one arrival, typically the first.

Finally, HWT is similar to WC in that both compute each wavefront from the preceding one. However, WC involves ray tracing from one wavefront to the next, while in HWT one wavefront is generated from the preceding by finite-differences in the ray domain.

CONCLUSIONS AND FUTURE WORK

My extension of Huygens wavefront tracing to three dimensions retains the benefits offered by the method in two dimensions, namely its stability in regions of high velocity contrast, its accuracy, and its computational efficiency.

As for any other traveltime method that involves computations in the ray domain, the interpolation to a Cartesian grid remains the major problem. In the current implementation, the interpolation is about one order of magnitude more expensive than the traveltime computation itself.

A possible direction for future work is to modify HWT to a grid-adaptive finite-difference method. HWT requires computing derivatives along the wavefronts. As the distance be-

tween adjacent points on the wavefront increases, the accuracy of those derivatives decreases. One possible way to increase the accuracy is to adapt the sampling of the wavefront in the ray domain, as done with finite-difference methods in the physical domain (Symes et al., 1999).

ACKNOWLEDGEMENTS

I would like to thank Bill Symes for many useful discussions. I also wish to thank James Rickett for the support in generating the wave-equation modeling examples.

REFERENCES

Červený, V., 1987, Ray tracing algorithms in three-dimensional laterally varying layered structures: Seismic Tomography, 99–134.

Fomel, S., 1997, A variational formulation of the fast marching eikonal solver: SEP–**95**, 127–147.

Nichols, D., Farmer, P., and Palacharla, G., 1998, Improving prestack imaging by using a new ray selection method: 68th Annual Internat. Mtg., Soc. Expl. Geophys., Expanded Abstracts, 1546–1549.

Popovici, A. M., and Sethian, J., 1997, Three-dimensional traveltime computation using the fast marching method: 67th Annual Internat. Mtg., Soc. Expl. Geophys., Expanded Abstracts, 1778–1781.

Sava, P., and Biondi, B., 1997, Multivalued traveltime interpolation: SEP–**95**, 115–126.

Sava, P. C., and Fomel, S., 1998, Huygens wavefront tracing: A robust alternative to ray tracing: 68th Annual Internat. Mtg., Soc. Expl. Geophys., Expanded Abstracts, 1961–1964.

Symes, W. W., Belfi, C. S., and Qian, J., 1999, Adaptive grid eikonal solvers: 5th SIAM Conference on Mathematical and Computational Issues in the Geosciences, 90.

van Trier, J., and Symes, W. W., 1991, Upwind finite-difference calculation of traveltimes: Geophysics, **56**, no. 6, 812–821.

Vidale, J. E., 1990, Finite-difference calculation of traveltimes in three dimensions: Geophysics, **55**, no. 5, 521–526.

Vinje, V., Iversen, E., and Gjoystdal, H., 1993, Traveltime and amplitude estimation using wavefront construction: Geophysics, **58**, no. 8, 1157–1166.